A Spectral Element Method for Oldroyd-B Fluid in a Contraction Channel

Sha Meng, Xin Kai Li, and Gwynne Evans

Institute of Simulation Sciences,
Faculty of Computing Science and Engineering,
De Montfort University, Leicester LE1 9BH, England
smeng@dmu.ac.uk, xkl@dmu.ac.uk, gaevans@dmu.ac.uk
http://www.cse.dmu.ac.uk/ISS/

Abstract. A spectral element method coupled with the EVSS method for computing viscoelastic flows is presented. The nonlinear rheological model, Oldroyd-B, is chosen to simulate the flow of a viscoelastic fluid based on a planar four-to-one abrupt contraction benchmark problem. Numerical results agree well with those in the previous publications.

Keywords: Viscoelastic flow; Spectral element method; Oldroyd-B fluid

1 Introduction

Non-Newtonian fluids, such as multi-grade oils, liquid detergents, polymer melts and molten plastics, are becoming more and more important in many industrial fluids applications. Viscoelastic fluids are non-Newtonian fluids that possess memory. That is, the stress of the fluid depends not only on the stresses actually impressed on them at present, but also on all the stresses to which they have been subjected during their previous deformation history. These fluids are special case of non-Newtonian fluids that lie somewhere in between elastic materials and standard Newtonian fluids. The numerical simulation of such viscoelastic fluids is becoming an effective technique to predict the fluid performance in a wide range of engineering applications.

Most mathematical problems that arise in modeling viscoelastic flows involve the solutions of non-linear partial differential, integro-differential or integral equations. In general, these equations cannot be solved analytically, so numerical methods are required to obtain solutions. The rapid growth in the power and availability of computers has led to the development of many algorithms for solving these equations. Recently, the spectral element method has emerged in the viscoelastic context as a powerful alternative to more traditional methods in predicting flow behaviour in complex fluids. In this paper we mainly focus on the development of an efficient spectral element technique to simulate a viscoelastic flow in a contraction channel.

Contraction flows of viscoelastic fluids are of importance in fundamental flow property measurements as well as in many industrial applications [1]. The theoretical prediction of entry-flow for non-Newtonian fluids still is a difficult task.

V.N. Alexandrov et al. (Eds.): ICCS 2001, LNCS 2073, pp. 852–861, 2001.
© Springer-Verlag Berlin Heidelberg 2001

The difficulty comes from two aspects. One is the constitutive equations that are used to express the relationship between the stress tensor and the velocity gradient and describe the rheological behaviour of viscoelastic fluids which have memory effects and contain nonlinear terms that add to the complexity of the problem; the other one is a geometrical singularity at the re-entrant corner. The research has been dominated by the study of the high Weissenberg numbers and continues to be a benchmark problem in the computational rheology.

In recent years, successful numerical methods have emerged. These include the Hermitian finite element method [7], the 4×4 subelement method [8], the explicitly elliptic momentum equation formulation (EEME) [5], the elastic viscous split stress formulation (EVSS) [10], the consistent streamline upwind Petrov-Galerkin method (SUPG) [4] and the discontinuous Galerkin (DG) method [3]. In this paper, we will present a spectral element formulation to solve the Oldroyd-B viscoelastic flow based on a four-to-one contraction benchmark problem. In section 2, the full set of governing equations for the viscoelastic flow model is presented. The spectral element method is described in section 3, numerical results and discussion are presented in the last section.

2 Mathematical Modeling

The isothermal flow of an incompressible viscoelastic fluid is governed by a set of conservation and constitutive equations. In the absence of body force, the momentum and mass equations can be written as follows

$$\rho\left(\frac{\partial \mathbf{u}}{\partial t}+\mathbf{u}\cdot\nabla\mathbf{u}\right)=-\nabla p+\nabla\cdot\boldsymbol{\tau}, \tag{2.1}$$

$$\nabla\cdot\mathbf{u}=0, \tag{2.2}$$

where ρ is the fluid density, p is the pressure, $\mathbf{u}$ is the velocity vector, and $\boldsymbol{\tau}$ is the extra-stress tensor field. Equations (2.1) and (2.2) must be closed with a constitutive model. In this paper, the Oldroyd-B model is used and defined as

$$\boldsymbol{\tau}+\lambda_1\overset{\nabla}{\boldsymbol{\tau}}=2\eta(\mathbf{D}+\lambda_2\overset{\nabla}{\mathbf{D}}), \tag{2.3}$$

where λ_1 is the relaxation time, λ_2 is the retardation time and η is the shear rate viscosity. $\mathbf{D}$ and $\overset{\nabla}{\boldsymbol{\tau}}$ are the rate of deformation tensor and the upper-convected derivative of the viscoelastic extra-stress, respectively. They are defined as

$$\mathbf{D}=\frac{1}{2}(\nabla\mathbf{u}+(\nabla\mathbf{u})^T),$$

$$\overset{\nabla}{\boldsymbol{\tau}}=\frac{\partial\boldsymbol{\tau}}{\partial t}+\mathbf{u}\cdot\boldsymbol{\nabla}\boldsymbol{\tau}-\boldsymbol{\tau}\cdot(\nabla\mathbf{u})-(\nabla\mathbf{u})^T\cdot\boldsymbol{\tau}.$$

Note that equation (2.3) reduces to the upper-convected Maxwell (UCM) model if $\lambda_2=0$ and to a Newtonian liquid with viscosity η if $\lambda_1=\lambda_2$. The viscoelastic stress tensor can be split into

$$\boldsymbol{\tau}=\boldsymbol{\tau}_1+\boldsymbol{\tau}_2, \tag{2.4}$$

where $\boldsymbol{\tau}_1$ denotes the elastic part of the viscoelastic stress defined as

$$\boldsymbol{\tau}_1 + \lambda \overset{\nabla}{\boldsymbol{\tau}}_1 = 2\eta_1 \mathbf{D},$$

and $\boldsymbol{\tau}_2$ represents the purely viscous component defined as

$$\boldsymbol{\tau}_2 = 2\eta_2 \mathbf{D}.$$

in these equations η_1 is the viscosity of the viscoelastic contribution and η_2 is the viscosity of the Newtonian contribution.

Substituting (2.4) into (2.3), we obtain the Oldroyd-B constitutive equation

$$\boldsymbol{\tau}_1 + \lambda_1 \left(\frac{\partial \boldsymbol{\tau}_1}{\partial t} + \mathbf{u} \cdot \boldsymbol{\nabla} \boldsymbol{\tau}_1 - \boldsymbol{\tau}_1 \cdot (\nabla \mathbf{u}) - (\nabla \mathbf{u})^T \cdot \boldsymbol{\tau}_1 \right) = \eta_1 (\nabla \mathbf{u} + (\nabla \mathbf{u})^T). \quad (2.5)$$

Let $\mathbf{d}$ be an additional unknown

$$\mathbf{d} = \mathbf{D} = \frac{\mathbf{1}}{\mathbf{2}} (\nabla \mathbf{u} + (\nabla \mathbf{u})^{\mathbf{T}}),$$

and replace $\boldsymbol{\tau}_1$ by $\boldsymbol{\tau}$, we obtain $(\mathbf{u}, p, \boldsymbol{\tau}, \mathbf{d})$ in the EVSS formulation

$$\rho \left(\frac{\partial \mathbf{u}}{\partial t} + \mathbf{u} \cdot \nabla \mathbf{u} \right) = -\nabla p + \nabla \cdot \boldsymbol{\tau} - 2\eta_1 \nabla \cdot \mathbf{d} + \mathbf{2}\eta \nabla \cdot \mathbf{D}, \quad (2.6)$$

$$\nabla \cdot \mathbf{u} = 0, \quad (2.7)$$

$$\boldsymbol{\tau} + \lambda_1 \overset{\boldsymbol{\nabla}}{\boldsymbol{\tau}} = 2\eta_1 \mathbf{D}, \quad (2.8)$$

$$\mathbf{d} = \mathbf{D}. \quad (2.9)$$

Although we add the same quantity in the right hand side of the momentum equation, the real modification will be appear when we consider different representations for $\mathbf{d}$ and $\mathbf{D}$ in the discrete form of the above system of equations. Furthermore, a dimensionless system of equations can be written as

$$Re \left(\frac{\partial u_i}{\partial t} + u_j \frac{\partial u_i}{\partial x_j} \right) = -\frac{\partial p}{\partial x_j} + \frac{\partial \tau_{ij}}{\partial x_j} - 2(1-\beta) \frac{\partial d_{ij}}{\partial x_j} + \frac{\partial^2 u_i}{\partial x_j^2}, \quad (2.10)$$

$$\frac{\partial u_i}{\partial x_i} = 0, \quad (2.11)$$

$$\tau_{ij} + We \left(\frac{\partial \tau_{ij}}{\partial t} + u_l \frac{\partial \tau_{ij}}{\partial x_l} \right) = (1-\beta) \left(\frac{\partial u_i}{\partial x_j} + \frac{\partial u_j}{\partial x_i} \right) + We \left(\tau_{il} \frac{\partial u_j}{\partial x_l} + \tau_{jl} \frac{\partial u_i}{\partial x_l} \right), \quad (2.12)$$

$$d_{ij} = \frac{1}{2} \left(\frac{\partial u_i}{\partial x_j} + \frac{\partial u_j}{\partial x_i} \right), \ \forall\, i, \ \ j, \ \ l = 1, \ \ 2, \quad (2.13)$$

where $Re = \frac{\rho U L}{\eta}$ is the Reynolds number, $We = \frac{\lambda_1 U}{L}$ is the Weissenberg number, and $\beta = \frac{\lambda_2}{\lambda_1}$, which determines the characteristics of the Oldroyd-B fluid.

3 The Spectral Element Discretization

The spectral element method is a high-order weighted-residual technique for partial differential equations that combines the rapid convergence rate of the p-type spectral method with the geometric flexibility of the h-type finite element technique. In the spectral element discretization, the computational domain is broken into macro-spectral elements, and the dependent and independent variables are represented as high-order orthogonal polynomial expansions within the individual subdomains. Variational projection operators and Gauss-Lobatto Legendre numerical quadratures are used to generate the discrete equations, which are then solved by direct or iterative procedures using tensor-product sum-factorization techniques [6].

In order to obtain a weak formulation which is equivalent to the equations $(2.10) - (2.13)$, we introduce the following function spaces:

$$H_0^1(\Omega) = \{\phi : \phi \in H^1(\Omega), \phi = 0 \text{ on } \partial\Omega\},\ L_0^2(\Omega) = \{v : v \in L^2(\Omega), v = 0 \text{ on } \partial\Omega\},$$

where $H^1(\Omega)$ is Soblev space, $L^2(\Omega)$ is the space of square integrable functions. The scalar product can be defined as

$$(\phi, \psi) = \int_\Omega \phi(x)\psi(x)dx,\ \ \forall \phi, \psi \in H^1(\Omega).$$

The spectral element discretization proceeds by breaking up the computational domain Ω into K non-overlapping sub-domains denoted by $\Omega_k, (k = 1, ..., K)$ such that $\Omega = \cup\Omega_k, \forall k, l, k \neq l, \Omega_k \cap \Omega_l = \emptyset$. Each physical element is mapped onto the parent element $\chi^2 = [-1, 1] \times [-1, 1]$, on which a Gauss-Lobatto-Legendre grid is used. We further define

$$X_h = \{u : u|_\Omega \in P_N(\Omega)\} \cap H_0^1(\Omega),\ \ M_h = \{p : p|_\Omega \in P_{N-2}(\Omega)\} \cap L_0^2(\Omega),$$

where $P_N(\Omega)$ denotes the space of all polynomials of degree N or less. It is well known that a choice for the velocity in X_h and the pressure in M_h above avoids spurious pressure nodes and satisfies generalized the Brezzi-Babuska condition [2]. In addition, the second compatibility condition needs to be satisfied for the stress and the rate of deformation tensor spaces. In this paper, we choose $T_h = X_h$ and $D_h = M_h$ in order to have a well-posed solution. Then the spectral element discretization is:
Find $u_{i,h} \in X_h$, $p_h \in M_h$, $\tau_{ij,h} \in T_h$ and $d_{ij,h} \in D_h$ such that

$$\left(\frac{\partial u_{i,h}}{\partial x_j}, \frac{\partial \bar{u}_i}{\partial x_j}\right)_{h,GL} + Re\left(\frac{\partial u_{i,h}}{\partial t}, \bar{u}_i\right)_{h,GL} - \left(p_h, \frac{\partial \bar{u}_i}{\partial x_j}\right)_{h,GL} = \left(\frac{\partial \tau_{ij,h}}{\partial x_j}, \bar{u}_i\right)_{h,GL}$$

$$-2(1-\beta)\left(\frac{\partial d_{ij,h}}{\partial x_j}, \bar{u}_i\right)_{h,GL} - Re\left(u_{j,h}\frac{\partial u_{i,h}}{\partial x_j}, \bar{u}_i\right)_{h,GL}, \tag{3.1}$$

$$\left(\frac{\partial u_{i,h}}{\partial x_i}, q\right)_{h,GL} = 0, \tag{3.2}$$

$$We\left(\frac{\partial \tau_{ij,h}}{\partial t}+u_{l,h}\frac{\partial \tau_{ij,h}}{\partial x_l},\bar{\tau}_{ij}\right)_{h,GL}-We\left(\tau_{il,h}\frac{\partial u_{j,h}}{\partial x_l}+\tau_{jl,h}\frac{\partial u_{i,h}}{\partial x_l},\bar{\tau}_{ij}\right)_{h,GL}$$

$$+(\tau_{ij,h},\bar{\tau}_{ij})_{h,GL}=(1-\beta)\left(\frac{\partial u_{i,h}}{\partial x_j}+\frac{\partial u_{j,h}}{\partial x_i},\bar{\tau}_{ij}\right)_{h,GL}, \tag{3.3}$$

$$\left(d_{ij,h},\bar{d}_{ij}\right)_{h,GL}=\frac{1}{2}\left(\frac{\partial u_{i,h}}{\partial x_j}+\frac{\partial u_{j,h}}{\partial x_i},\bar{d}_{ij}\right)_{h,GL}, \tag{3.4}$$

$$\forall \bar{u}_i\in X_h,\ \ \forall q\in M_h,\ \ \forall \bar{\tau}_{ij}\in X_h,\ \ \forall \bar{d}_{ij}\in M_h,\ \ \forall i,\ j,\ l=1,\ 2,$$

where $(*,*)_{h,GL}$ refers to Gauss-Lobatto quadrature which is defined as

$$(f,g)_{h,GL}=\sum_{k=1}^{K}\sum_{m=0}^{M}\sum_{n=0}^{N}\rho_m\rho_n f(\xi_m^k,\phi_n^k)g(\xi_m^k,\phi_n^k)J^k,$$

where ξ_m^k, ϕ_n^k are the locations of the local nodes $\{m;k\}$, $\{n;k\}$ respectively, ξ_m,ϕ_n are the Gauss-Lobatto-Legendre quadrature points, and ρ_m,ϕ_n are the Gauss-Lobatto-Legendre quadrature weights, J^k is the transformation Jacobian on each element.

In this paper we use the Gauss-Lobatto-Legendre polynomials as a basis to span the approximation space X_h and T_h, which is defined as

$$h_i(\xi)=-\frac{1}{N(N+1)L_N(\xi_i)}\frac{(1-\xi^2)L_N^{'}(\xi)}{\xi-\xi_i},\ \ \xi\in[-1,1],\ \ \forall i\in\{0,...,N\},$$

where L_N is the Legendre polynomial of order N, the points ξ_i are the collocation points on the Gauss-Lobatto-Legendre grid. Therefore, the velocity and the stress tensor approximations in the parent element corresponding to element Ω_k are

$$u_h^k(\xi,\phi)=\sum_{p=0}^{M}\sum_{q=0}^{N}u_{pq}^k h_p(\xi)h_q(\phi), \tag{3.5}$$

$$\tau_h^k(\xi,\phi)=\sum_{p=0}^{M}\sum_{q=0}^{N}\tau_{pq}^k h_p(\xi)h_q(\phi), \tag{3.6}$$

where $u_{pq}^k=u(\xi_p^k,\phi_q^k)$, $\tau_{pq}^k=\tau(\xi_p^k,\phi_q^k)$. If we consider the velocity-pressure formulation, it is well known that the mixed interpolations must satisfy a compatibility condition. The framework of the spectral element method [6] has shown that a suitable choice for the pressure approximation space is M_h when the velocity is X_h. Therefore, in this paper, we choose the pressure function in the space M_h and expand it on the interior Gauss-Lobatto-Legendre points as shown in Fig. 1. Thus the pressure approximation can be written as

$$p_h^k(\xi,\phi)=\sum_{p=1}^{M-1}\sum_{q=1}^{N-1}p_{pq}^k\bar{h}_p(\xi)\bar{h}_q(\phi), \tag{3.7}$$

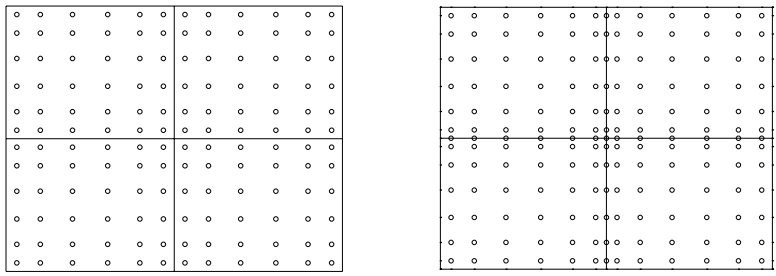

Fig. 1. Spectral element configurations ($K = 4, M = N = 5$). (a) Interior Gauss-Lobatto-Legendre collocation points for the pressure and the deformation tensor. (b) Gauss-Lobatto-Legendre collocation points for the velocity and the stress.

where $p_{pq}^k = p(\xi_p^k, \phi_q^k)$, $\bar{h}_p$ is defined as

$$\bar{h}_p = -\frac{(1-\xi_p^2)L_N^{'}(\xi)}{N(N+1)L_N(\xi_p)(\xi-\xi_p)}, \quad \xi \in [-1,1], \quad \forall p \in \{1,...,N-1\}.$$

Similarly, we define the approximation of the deformation tensor as

$$d_h^k(\xi,\phi) = \sum_{p=1}^{M-1}\sum_{q=1}^{N-1} d_{pq}^k \bar{h}_p(\xi)\bar{h}_q(\phi), \tag{3.8}$$

where $d_{pq}^k = d(\xi_p^k, \phi_q^k)$.

The velocity, pressure, stress and deformation tensor expansions $(3.5) - (3.8)$ are now inserted into equations $(3.1) - (3.4)$ and the discrete equations are generated by choosing appropriate test functions $\bar{\mathbf{u}}$ and $\bar{\boldsymbol{\tau}}$ in X_h whose values at a point (ξ_p, ϕ_q) are unity and zero at all other Gauss-Lobatto-Legendre points, and test functions q and $\bar{\mathbf{d}}$ in M_h whose values are unity at point (ξ_p, ϕ_q) and zero at all other interior Gauss-Lobatto-Legendre points. In this way we obtain the system of algebraic equations

$$A\mathbf{u} - B^T p = f,$$

$$-B \cdot \mathbf{u} = 0,$$

$$C\boldsymbol{\tau} = g,$$

$$E\mathbf{d} = h,$$

where A is the discrete Helmholtz operator, B is the discrete gradient operator, C is the stress tensor matrix, E is the deformation tensor matrix, f, g, h are the right hand side vectors, which are incorporated with boundary conditions.

4 The Decoupling Algorithm

Now for each time step, the algorithm consists of the following steps: Given an initial approximation $(u_i^0, p^0, \tau_{ij}^0, d_{ij}^0)$,

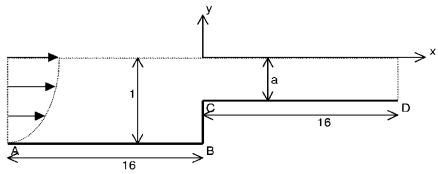

Fig. 2. The four-to-one planar contraction flow geometry.

Step 1: calculate the pressure p^n from the conservation equation by the Uzawa method [6].

Step 2: calculate the velocity $\mathbf{u}^n$ from the momentum equation using the stress $\boldsymbol{\tau}^{n-1}$ obtained from a previous iteration.

Step 3: calculate the stress $\boldsymbol{\tau}^n$ from the constitutive equation using $\mathbf{u}^n$.

Setp 4: calculate the deformation tensor $\mathbf{d}^n$ using the velocity field $\mathbf{u}^n$.

Step 5: check the convergence and return to step 1 if necessary.

5 Numerical Results

In this section, numerical results are presented for a four-to-one abrupt planar contraction. We adopt the ratio $\beta = \frac{1}{9}$ in order to compare with already published results. The difficulty of the four-to-one planar contraction problem is the existence of a singular solution which is caused by the geometric singularity at the re-entrant corner. The singularity in the viscoelatic flow is stronger than in the Newtonian flow.

Since the geometry is assumed to be symmetric about the central line, we need only consider the lower half of the channel. Fig. 2 shows the flow geometry. The height of the inflow half channel is taken as unity and the height of outflow channel is taken to be $a = \frac{1}{4}$. The length of inflow channel is taken to be 16 as is the length of outflow channel. Define $U = 1$ and $L = 1$, where U is the average velocity in the downstream half channel and L is the width of the downstream half channel, which gives $We = \lambda_1$.

We assume the fully developed Poiseuille flow at the inlet and outlet, the no-slip condition, $u = v = 0$, is applied on the solid boundaries, and $v = 0$ and $\frac{\partial u}{\partial y} = 0$ on the axis of symmetry. The boundary conditions for the stresses along the solid boundaries and inlet are derived from the steady state constitutive equations. At the exit we have Neumann boundary conditions for the stress variables

$$\frac{\partial \tau_{xx}}{\partial x} = \frac{\partial \tau_{yy}}{\partial x} = \frac{\partial \tau_{xy}}{\partial x} = 0.$$

Two different meshes depicted in Fig. 3 were used in the numerical simulations. Mesh1 consists of 5 elements, on each element there are 12 collocation points in the x-direction and 4 collocation points in the y-direction. Mesh2 has 3 elements, there are 18 collocation points in the x-direction and 6 collocation points in the y-direction on each element. We can see that the meshes created by the spectral element method are non-uniform, being refined near the re-entrant corner singularity.

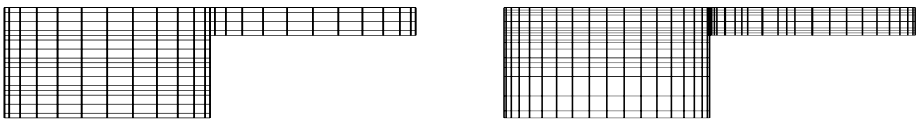

Fig. 3. Meshes for the four-to-one planar contraction problem: (a) Mesh1; (b) Mesh2.

The numerical stability has been tested for the Newtonian flow ($\lambda_1 = 0$) based on a $(\mathbf{u}, p, \boldsymbol{\tau}, \mathbf{d})$ formulation and numerical results agree well with the corresponding calculation by the velocity-pressure formulation. Fig. 4 shows contours of the stream function and the velocity profiles.

Now we consider the calculations in the viscoelastic case. The results on all the meshes have been computed with $\Delta t = 0.001$ and $Re = 1$. The length of the salient corner vortex L_1, the width of the salient corner vortex L_2 and the maximum value of the stream function φ_{max} are shown in Table 1 for We from 0.1 to 1.2. We found that when We increases from 0 to 0.6, the length of the corner vortex, L_1, is constant, while the width of the corner vortex, L_2, is increased. But when We increases from 0.7 to 1.2, L_1 decreases slightly, and L_2 remains constant. The size of corner vortex compares well quantitatively with the results of [9,11]. Contour plots of vorticity for $We = 0.1, 0.4, 0.8, 1.0$ in Mesh1 are shown in Fig. 5. These vorticity plots show that our numerical results are in good agreement with those obtained by [11].

The streamlines are plotted in Fig. 6 for $We = 0.1, 0.4, 0.8, 1.0$. In Fig. 7 the values of total stress components τ_{xy}, τ_{xx} and τ_{yy} along the line $y = -1$ are given for $We = 0.1, 0.4, 0.8, 1.0$. The maximum values of τ_{xy} and τ_{yy} at the corner are slightly increased when the value of We is increased. A huge increase occurs in the value of τ_{xx} from approximately 4.5 when $We = 0.1$, to approximately 49 when $We = 1.0$.

All accurate results have been presented up to $We = 1.2$. Since for high We number, it becomes more difficult to obtain fully developed velocity and stress fields, further work needs to be done in this area.

Table 1. Values of L_1, L_2 and φ_{max} for various We number with Mesh1.

We	L_1	L_2	φ_{max}
0.1	1.3093	1.086	1.0010672
0.2	1.3093	1.108	1.0010955
0.3	1.3093	1.129	1.0011469
0.4	1.3093	1.140	1.0011860
0.5	1.3093	1.151	1.0012160
0.6	1.3093	1.151	1.0012207
0.7	1.229	1.162	1.0012093
0.8	1.229	1.173	1.0012238
0.9	1.229	1.173	1.0012011
1.0	1.229	1.173	1.0011356
1.1	1.176	1.173	1.0010624
1.2	1.176	1.173	1.0009739

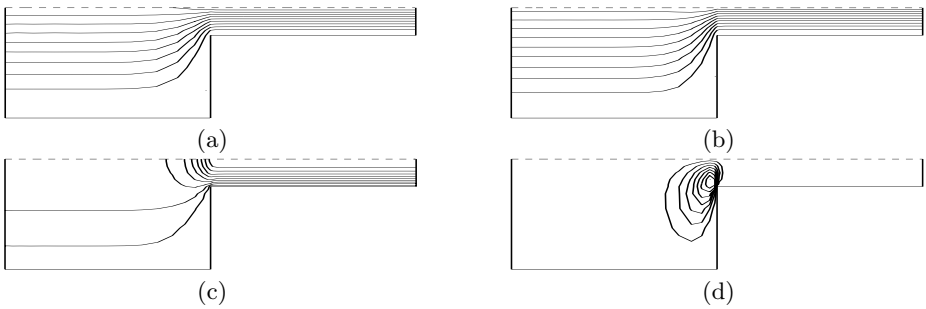

Fig. 4. Numerical stability for the Newtonian flow: (a) streamlines with Mesh1; (b) streamlines with Mesh2; (c) velocity profile in the x-direction with Mesh2; (d) velocity profile in the y-direction with Mesh2.

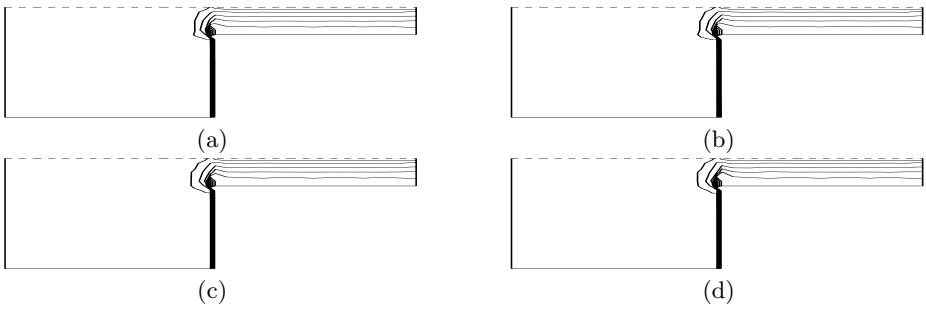

Fig. 5. Vorticity plots for increasing values of We for the viscoelastic flow problem with Mesh1: (a) $We = 0.1$; (b) $We = 0.4$; (c) $We = 0.8$; (d) $We = 1.0$.

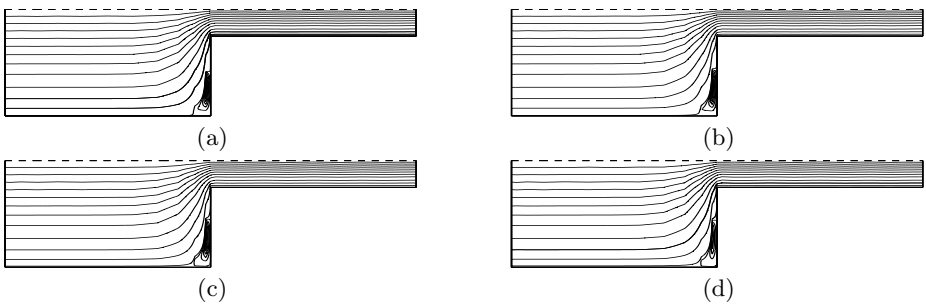

Fig. 6. Streamlines for increasing values of We for the viscoelastic flow problem with Mesh1: (a) $We = 0.1$; (b) $We = 0.4$; (c) $We = 0.8$; (d) $We = 1.0$.

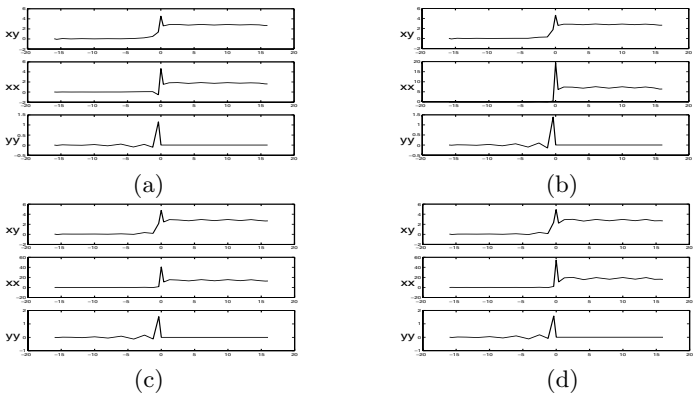

Fig. 7. The values of τ_{xy}, τ_{xx} and τ_{yy} along the line $y = -1$ for increasing values of We for the viscoelastic flow problem with Mesh1: (a) $We = 0.1$; (b) $We = 0.4$; (c) $We = 0.8$; (d) $We = 1.0$.

Acknowledgements
Sha Meng acknowledges the financial support of Ph.D studentship of De Montfort University.

References

1. D. V. Boger. Viscoelastic flows through contractions. *Ann. Rev. Fluid Mech.*, 19:157 182, 1987.
2. F. Brezza. On the existence: uniqueness and approximation of saddle-point problems arising from Lagrange multipliers. *RAIRO Anal. Numer.*, 8 R2:129 151, 1974.
3. M. Fortin and A. Fortin. A new approach for the FEM simulation of viscoelastic flows. *J. Non-Newtonian Fluid Mech.*, 32:295 310, 1989.
4. T. J. R. Hughes. Recent progress in the development and understanding of SUPG methods with special reference to the compressible Euler and Navier-Stokes equations. *Int. J. Num. Methods Fluids*, 7:1261 1275, 1987.
5. R. C. King, M. R. Apelian, R. C. Armstrong, and R. A. Brown. Numerical stable nite element techniques for viscoelastic calculations in smooth and singular geometries. *J. Non-Newtonian Fluid Mech.*, 29:147 216, 1988.
6. Y. Maday and A. T. Patera. Spectral element methods for the incompressible Navier-Stokes equations. *in State of the Art Surveys in Computational Mechanics*, pages 71 143, 1989.
7. J. M. Marchal and M. J. Crochet. Hermitian nite elements for calculating viscoelastic flow. *J. Non-Newtonian Fluid Mech.*, 20:187 207, 1986.
8. J. M. Marchal and M. J. Crochet. A new mixed nite element for calculating viscoelastic flow. *J. Non-Newtonian Fluid Mech.*, 26:77 115, 1987.
9. H. Matallah, P. Townsend, and M. F. Webster. Recovery and stress-splitting schemes for viscoelastic flows. *J. Non-Newtonian Fluid Mech.*, 75:139 166, 1998.
10. D. Ralagopalan, R. C. Armstrong, and R. A. Brown. Finite element methods for calculation of steady, viscoelatic flow using constitutive equations with a Newtonian viscosity. *J. Non-Newtonian Fluid Mech.*, 36:159 192, 1990.
11. T. Sato and S. M. Richardson. Explicit numerical simulation of time-dependent viscoelastic flow problem by a nite element/ nite volume method. *J.Non-Newtonian Fluid Mech.*, 51:249 275, 1994.